

Integrating binding affinity and tonic signaling enables a rational CAR design for augmented T cell function

Markus Barden ,¹ Patrick Ronan Elsenbroich ,¹ Vivian Haas,² Moritz Ertelt,^{2,3} Philip Pervan,¹ Lukas Velas,⁴ Bence Gergely ,⁵ Árpád Szöör,⁵ Dennis Christoph Harrer,¹ Valerie Bezler,¹ Astrid Holzinger,¹ Rasmus Ulslev Wegener Friis,⁶ Gyorgy Vereb,⁷ Gerhard J Schütz,⁴ Clara T Schoeder,^{2,3,8} Andreas A Hombach ,⁹ Hinrich Abken¹

To cite: Barden M, Elsenbroich PR, Haas V, *et al.* Integrating binding affinity and tonic signaling enables a rational CAR design for augmented T cell function. *Journal for ImmunoTherapy of Cancer* 2024;**12**:e010208. doi:10.1136/jitc-2024-010208

► Additional supplemental material is published online only. To view, please visit the journal online (<https://doi.org/10.1136/jitc-2024-010208>).

Accepted 06 November 2024

ABSTRACT

Background The success of chimeric antigen receptor (CAR) T cell therapy for hematological malignancies has not yet translated into long-term elimination of solid tumors indicating the need for adequately tuning CAR T cell functionality.

Methods We leveraged a translational pipeline including biophysical characterization and structural prediction of the CAR binding moiety, evaluation of cellular avidity, synapse formation, T cell motility, and functional capacities under repetitive target challenge and in sustained tumor control.

Results As an example of clinical relevance, we derived a panel of anti-Her2 CARs covering a 4-log affinity range, all expected to target the same Her2 epitope. The same scFv mutations increased both antigen-specific affinity, cellular avidity, and antigen-independent “tonic” signaling; above a minimum threshold, raise in affinity translated into functional avidity in a non-linear fashion. In this case, replacement by amino acids of higher hydrophobicity within the scFv coincidentally augmented affinity, non-specific binding, spontaneous CAR clustering, and tonic signaling, all together relating to T cell functionality in an integrated fashion.

Conclusions Data emphasize that tonic signaling is not always due to the positive charge but can be driven by hydrophobic interactions of the scFv. CAR binding affinity above the threshold and tonic signaling are required for sustained T cell functionality in antigen rechallenge and long-term tumor control.

BACKGROUND

The disappointing failure of CAR T cell therapy in solid tumors is attributed to inefficient triggering of T cell effector functions indicated by weak amplification, limited persistence, and early loss of killing capacities.¹ Each individual CAR domain has the potential to impact the quality and duration of T cell triggering.² While the CAR binding domain is primarily selected with respect to targeting specificity, it critically determines

WHAT IS ALREADY KNOWN ON THIS TOPIC

⇒ Excessive activation in solid tumors impedes long-term CAR T cell function which is thought to be prevented by downtuning binding affinity. The relationship between antigen-triggered and antigen-independent tonic CAR signaling and how both translate to functional T cell capacities is not characterized.

WHAT THIS STUDY ADDS

⇒ CAR binding affinity alone does not determine T cell effector functions. Rather high affinity and cellular avidity above the minimum threshold, combined with elevated tonic signaling, produce adequate T cell capacity for expansion and tumor control.

HOW THIS STUDY MIGHT AFFECT RESEARCH, PRACTICE OR POLICY

⇒ Data highlight the mechanistic complexity of tonic signaling and suggest inclusion of additional variables, for example, hydrophobic interactions, into the equation when determining the CAR's tonic signaling capacities. Above threshold affinity/avidity combined with tonic signaling provides CAR T cells with augmented capacities to successfully eradicate solid tumors.

how antigen engagement translates into triggering T cell functions.

CAR signaling needs to pass a minimum threshold to enable cytotoxic T cell function; however, signaling far above threshold may render the CAR T cell dysfunctional, also known as “exhaustion”.³ Initial CAR signaling strength in response to target antigen seems to be mainly influenced by the CAR affinity, CAR expression level on the T cell, and antigen level on the target cell.^{4,5} Among this matrix of dependencies, only CAR affinity is thoroughly controlled by appropriate CAR design. CAR affinity contributes to the degree of T cell activation; there is a clear threshold



© Author(s) (or their employer(s)) 2024. Re-use permitted under CC BY-NC. No commercial re-use. See rights and permissions. Published by BMJ.

For numbered affiliations see end of article.

Correspondence to

Hinrich Abken;
hinrich.abken@ukr.de

in CAR affinity above which the T cell becomes activated⁶ and the binding strength seems to determine the T cell functional capacities.^{5,7} We previously reported an interdependency of CAR affinity and target antigen density for a panel of anti-human Erb-B2 receptor tyrosine kinase-2 (Her2) CAR binders.⁶

Her2 is a relevant target for adoptive CAR T cell therapy since it is broadly expressed by a variety of carcinomas of different organs including breast, ovarian and colorectal cancer. In recent years, clinical trials have been initiated to evaluate Her2 CAR T cells for the treatment of solid cancers, including breast cancer (NCT04430595), pancreatic cancer (NCT01935843), lung cancer (NCT03198052), ovarian cancer (NCT04511871), rhabdomyosarcoma (NCT00902044),⁸ and CNS tumors, the latter with either systemic (NCT02442297, NCT03696030) or locoregional application (NCT03500991).⁹ However, comparison of the trial results is challenging since different anti-Her2 CARs with different binding moieties are used.

Like several other “tumor associated antigens”, Her2 is also expressed by healthy epithelia, although at far lower levels. In a fatal case of colon cancer treatment, anti-Her2 CAR T cells caused a cytokine release syndrome and infiltrated the lung which subsequently led to respiratory failure.¹⁰ In this situation, reducing the affinity to a level where CAR signaling strength is directly above the activation threshold could reduce the risk of CAR T cell-induced side effects while retaining antitumor capacities.¹¹ Reduced affinity CARs are currently in early clinical testing (NCT02443831).^{12,13} However, such “affinity-tuning” remains challenging and empirical as affinity often does not translate in a linear fashion to activation strength⁵ and triggering T cell effector functions is controlled by multiple dependencies. Adding to this matrix of dependencies, the scFv moiety is also involved in antigen-independent, tonic CAR signaling, which is defined as a low-level, constitutive signaling caused by mild autoclustering of CARs on the T cell membrane.¹⁴ Each scFv region, that is, the framework, linker, and complementarity determining regions (CDR), can potentially contribute to protein aggregation due to instability, polarity, or antigen-unrelated binding. While CDRs primarily determine specific binding properties, they are likewise responsible for antigen-unrelated binding properties^{15,16} and can contribute to scFv instability.¹⁷ We accordingly observed that the Her2-specific C6.5 scFvs, initially studied by our group in the context of affinity tuning, harbor CDR mutations which alter non-specific binding properties of the scFv. Here, we engineered a panel of second generation CD28-CD3 ζ CARs based on the C6.5 antibody derived scFvs for functional testing. Within the matrix of dependencies controlling T cell effector functions, we addressed whether integrating antigen-triggered signaling with antigen-unrelated tonic signaling results in CAR T cells with optimized functional capacities. We revealed that antigen triggering and tonic signaling are integrated into CAR T cell functional avidity,

and, within certain limits, lead to augmented anti-tumor capacities.

METHODS

Three-dimensional structure prediction, molecular dynamics simulations

The structure of all scFvs was predicted with AlphaFold2.¹⁸ The solution builder of CHARMM-GUI¹⁹ was used for system solvation with TIP3P water molecules, and charge was neutralized with NaCl. All simulations used the Amber ff19sb force field.²⁰ The calculations were performed with the Amber molecular dynamics (MDs) package through the pmemd software.²¹ After an initial minimization step, Langevin dynamics with a friction coefficient of 1 ps⁻¹ were applied for linear heating of the system in constant volume for 1 ns, during which the protein was positionally restrained with a final equilibrium temperature of 310.15 K. Next, an NPT simulation was performed using the Monte Carlo barostat to control the isotropic pressure scaling (N denotes the constant particle number, P equals pressure and T temperature). For electrostatic interactions a long-distance cut-off of 9 Å was applied. For each scFv, three 1000 ns long simulations were performed. The resulting trajectories were analyzed with pytraj,²² a python package binding of cpptraj.²³

Binding assays

The C6.5 derived scFv-Fc panel and 6xHis-tagged Her2 were expressed in Expi293 cells and purified using affinity and desalting chromatography or size-exclusion chromatography (HiTrap MabSelect Prisma protein A column; HisTrap excel; HiPrep 26/10 Desalting; HiLoad 16/600 Superdex, Cytiva, Marlborough, Massachusetts, USA) in an ÄKTA system (Cytiva, Marlborough, Massachusetts, USA), respectively.

For kinetic analysis, Octet ProA Biosensors (Octet R8, Sartorius, Göttingen, Germany) were used to load the respective scFvs (5 μ g/mL). Association to Her2 was measured in dilution series in HBS-EP+buffer which was also used as reference at 37°C. Binding kinetics were analyzed with the Octet biolayer interferometry (BLI) analysis software (V.12.2), performing subtraction of the reference, Y axis alignment, and Savitzky-Golay filtering.

For ELISA, 384-well high-binding plates (Greiner, Kremsmünster, Austria) were coated with antigen at a concentration of 10 μ g/mL (Her2, heparin, bovine serum albumin (BSA)) or 50 μ g/mL (cardiolipin). After blocking, serially diluted scFvs were added in triplicate. Detection of binding was achieved through addition of anti-human IgG antibodies conjugated with horseradish peroxidase (polyclonal, SouthernBiotech, Birmingham, Alabama, USA) and TMB reagent, recording the absorption at 450 nm. Data were normalized to a control included on each plate,

and the percentage of non-specific binding was calculated in reference to specific Her2 binding.

T cell modification and functional assays

CAR T cells were engineered by transduction of T cells with gamma-retroviruses encoding the respective CAR as described.²⁴

NFAT activation was recorded after 20 hours of stimulation via luminescence using CAR transduced Jurkat-Lucia NFAT cells (InvivoGen, Toulouse, France). Jurkat cells were co-incubated with uncoated wells (PBS, negative control), OKT3/15E8 antibody coated wells (positive control), or a serial dilution of “Recombinant Human Erb2/Her2 Fc Chimera Protein”, CF (R&D Systems, Minneapolis, USA) or goat anti-human IgG-UNLB antibody (polyclonal, SouthernBiotech) coated wells.

T cells were analyzed via flow cytometry using the following antibodies: anti-CD4 antibody (clone: M-T466, Miltenyi Biotec, Bergisch Gladbach, Germany), anti-CD8 antibody (clone: BW135/80, Miltenyi Biotec), goat F(ab')₂ anti-human IgG-PE antibody (clone: none, SouthernBiotech), anti-CD3 antibody (clone: OKT3, BioLegend, San Diego, California, USA), anti-FASL antibody (clone: NUK-1, BioLegend), anti-Annexin V antibody (clone: none, BD, Franklin Lakes, USA). The live/dead dye eFlour 780 (Thermo Fisher Scientific, Waltham, Massachusetts, USA) was used for detection of live cells. eFlour 450 proliferation dye (Thermo Fisher Scientific) was used to assess proliferative capacities.

For repetitive engagement with target cells (“stress test”), CAR T cells were initially co-incubated with SKOV3 and LS174T cells at an E:T ratio of 5:1 (100,000 CAR T cells to 20,000 tumor cells). After incubation for 3–4 days, 20% of the culture volume was used for flow cytometric analysis while the remaining 80% culture volume was transferred to a fresh well with 20,000 tumor cells. The number of remaining tumor cells and CAR T cells were quantified by flow cytometry using “AccuCheck Counting Beads” (Thermo Fisher Scientific). Assessment of CAR T cell survival without antigen or with CAR crosslinking via plate-coated 0.3 µg/mL goat anti-human IgG (polyclonal, SouthernBiotech) was performed in the same fashion as the “stress test”.

Cellular binding force assay

CAR-specific binding force was measured using the z-Movi device (Lumicks, Amsterdam, The Netherlands). SKOV3 cells were seeded onto microfluidic chips at a concentration of 5×10^7 cells per ml to obtain a confluent monolayer. MACS enriched (>95%) CAR⁺ T cells were labeled with “CellTrace Far Red” dye to enable T cell tracking. CAR of irrelevant specificity (CD30) was used as negative control. After co-incubation of CAR T cells and SKOV3 cells on the chip, a force ramp ranging from 0 to 1000 pN was applied for 2.5 min. T cell detachment was detected by fluorescence imaging. Binding force was analyzed by the Ocean software (V.1.0, Lumicks). Plateau force is defined as force value during force ramp whereby decrease of %

bound cells drops below 2% per force step and is calculated based on negative control CARs.

Total internal reflection fluorescence microscopy

Image acquisition was performed on a home-built setup comprised of an Olympus IX73 (Japan) microscope body equipped with a high NA objective (Carl Zeiss, Oberkochen, Germany, alpha-plan apochromat, 1.46 NA, 100×), 488 nm excitation laser (OBIS Laser box, Coherent, Mountain View, USA), a quad dichroic mirror (Di01-R405/488/532/635, Semrock, USA) and an emission filter (ZET405/488/532/642m, Chroma, Bellows Falls, USA). CAR-GFP T cells were incubated on Her2 protein-coated slides for 40 min prior to fixation and imaged by total internal reflection fluorescence (TIRF) microscopy on excitation at 488 nm. Data were analyzed by custom Python code (V.3.6) available on request from the corresponding author using the following libraries: numpy,^{25–27} mpl_toolkits, scipy, sdt, pandas, matplotlib, seaborn.

Confocal imaging of CAR surface distribution

Unstimulated CAR-GFP SupT1 cells were fixed using 1% paraformaldehyde in PBS for 30 min at room temperature and subsequently washed three times in PBS. The cells were mounted on glass slides using ProLong mounting medium (Thermo Fisher Scientific) and imaged using an LSM710 confocal laser microscope (Carl Zeiss). Acquired images were analyzed using the Zeiss Zen software V.3.1 (Carl Zeiss).

Confocal timelapse live video microscopy

3D live cell imaging was conducted on a Leica Stellaris 8 confocal microscope (Leica Microsystems, Wetzlar, Germany). 30,000 CAR T cells were co-cultured with 500,000 LS174T cells at 37°C, 95%–100% humidity and 5% CO₂ (Okolab, Rovereto, Italy). For image acquisition, an HC PL APO CS2 20x/0.75 DRY objective without confocal scanner zoom was used, resulting in a field of view of 582 µm xy-size. Z-stacks (30 images, 0.856 µm step size) were acquired in “line mode” with bidirectional scanning speed at 400 Hz; pinhole size was 76.1 µm. “CellTrace Far Red” labeled CAR T cells were imaged on excitation at 630 nm (0.2% intensity) and detection at 670/10 nm (10% gain). At each position, z-stacks were imaged every 5 min, resulting in 150 z-stacks in total for the entire duration of 12:30 hours. T cell objects were created by Imaris V.x64 9.9.1 software. Tracking was performed using the “autoregressive motion” algorithm. Subsequent analysis was performed with R V.4.2.1. For each CAR construct, the mean movement between any two adjacent points in time (measured with the Imaris statistic “cell displacement delta length”) was calculated for all 150 time points and overall tracked cells, resulting in a single mean motility value per CAR and donor. Mean motility was normalized per donor by dividing through the sum of all CARs.

Xenograft tumors and in vivo treatment

NSG (NOD.Cg-Prkdcscid/Il2rgtm1Wjl/SzJ) mice were purchased from The Jackson Laboratory and housed in

a specific pathogen-free environment. Power analysis was performed to define sample size. Animals were given a 7-day acclimatization period to adjust to environment and handling. Animals were allocated to different groups using a random number generator to ensure unbiased distribution. On day 0, each 7-week-old female NSG mouse participating in the study was given a subcutaneous injection in both flanks, each containing 3×10^6 N87.flLuc cells in 100 μ L PBS mixed with an equal volume of Matrigel (BD Biosciences, San Jose, California, USA). No animals or data points were excluded from the analysis. Tumor growth was monitored by blinded personnel using an IVIS Spectrum CT instrument (Perkin Elmer, Waltham, Massachusetts, USA). Before measurement, isoflurane-anesthetized animals were injected i.p. with D-luciferin (150 mg/kg). A bioluminescence image was obtained and analyzed after 10 min using “Living Image” software V.4.0 (Caliper Life Sciences, Waltham, Massachusetts, USA). Signal intensity measured as total photons per second per square centimeter per steradian ($p/(s \times cm^2 \times sr)$) was obtained from identically sized ROIs. Mice received on day 14 one intravenous dose of 5×10^5 NT (non-modified T cells) or Her2-specific CAR T cells (C6.5 or C6-B1D2 groups). Endpoint criteria were met when animals showed signs of severe distress, pain, or suffering that could not be alleviated in accordance with ethical guidelines and veterinary advice.

Statistical analysis

All statistical analyses were performed by using the Prism V.10 software (GraphPad), except for microscopic analyses as described above. A $p \leq 0.05$ was considered statistically significant.

RESULTS

C6.5 antibody derived anti-Her2 CARs differ in their binding affinities and primary activation capacities

To investigate how CAR triggered T cell functionality is altered by scFv mutations introduced for the purpose of affinity maturation, we used the anti-Her2 scFv panel that was previously generated by site-directed mutagenesis of the anti-Her2 scFv C6.5 (figure 1A) and covers a 4-log affinity range.²⁸ We engineered a series of anti-Her2 CARs of the same modular configuration (figure 1B). All CARs were expressed by the same vector at nearly the same level on the surface of engineered human T cells, thus enabling uncompromised functional studies. The anti-CD19 CAR of irrelevant specificity served as control (figure 1B).

We observed a clear minimum threshold in affinity in the response to Her2^{medium} LS174T target cells as measured by NFAT activation in an Jurkat-Lucia NFAT reporter assay (figure 1C, online supplemental figure 1); above that threshold, CAR T cell activation was initiated. The affinity threshold was overridden by engagement of Her2^{high} SKOV3 target cells, which triggered NFAT activation also through the low affinity C6.5G98A scFv

CAR (figure 1D). Above affinity threshold, all CARs likewise induced amplification of T cells on engagement of Her2 high and medium expressing cells (figure 1E,F), increased the proportion of central memory cells (figure 1G,H), induced FASL expression (figure 1I,J), and finally induced activation-induced cell death, as indicated by Annexin V staining (figure 1K,L). Interestingly, the CAR with the highest affinity was associated with a lower frequency of cell death than the medium affinity CARs.

Affinity tuning of the scFv impacts both antigen-specific and non-specific binding

Starting with the C6.5 scFv antibody, an alanine scan of the C6.5 V_H CDR3 produced the C6.5G98A scFv with reduced affinity (figure 2A).²⁸ A C6.5 V_L CDR3 library screen provided the C6ML3-9 scFv with increased affinity; C6.5 V_H CDR3 was mutated to further increase affinity resulting in the C6MH3-B1 as well as C6-B1D2 scFv.²⁸

To understand the affinity differences, we modeled the respective scFv structures using AlphaFold2 (figure 2B). The predicted structure of C6.5 and derived variants have a long V_H CDR3 loop containing a disulfide bridge, which is a major driver of the adopted conformation. The G98A mutation drastically reduces affinity, however, is not exposed. Taken together, we hypothesized that the V_H CDR3 loop flexibility is crucial for high affinity binding. We ran classical MDs simulations of the predicted structures of all variants and used principal component analysis to study conformational states (figure 2B). Interestingly, the C6.5 scFv adopted at least two distinct loop conformations, while this shift is missing on G98A mutation. The C6ML3-9 scFv had a smaller shift between the two V_H CDR3 loop conformations. The two highest affinity variants, C6MH3-B1 and C6-B1D2 scFv, had no large conformational shift of the V_H CDR3 loop. We concluded that affinity maturation seems to be due to stabilizing the V_H CDR3 loop in a favorable position that decreases the dissociation rate from Her2 antigen.

To transfer the previously determined scFv binding affinity to the CAR context, we used the respective scFv linked to IgG1 hinge-CH2-CH3 as it constitutes the extracellular CAR construct and assessed the binding properties by BLI. K_D values were not determined due to multivalent use of ligand and analyte. However, the differences in the dissociation rates were confirmed as for the reported scFvs without linked CAR domains. Given similar loading of the scFvs to the tips, the affinity panel was confirmed based on the maximum response on Her2 binding (figure 2C, online supplemental figure 2).

Introduction of more hydrophobic amino acids during the course of affinity maturation potentially also alters the non-specific scFv binding and turns the scFv toward a stickier one. Therefore, we analyzed non-specific binding of the scFv panel by ELISA using BSA, heparin, and cardiolipin as unrelated target proteins, and compared with Her2-specific binding. In the V_H CDR3 of C6-B1D2, amino acids were substituted from YFQH to WLGV resulting in

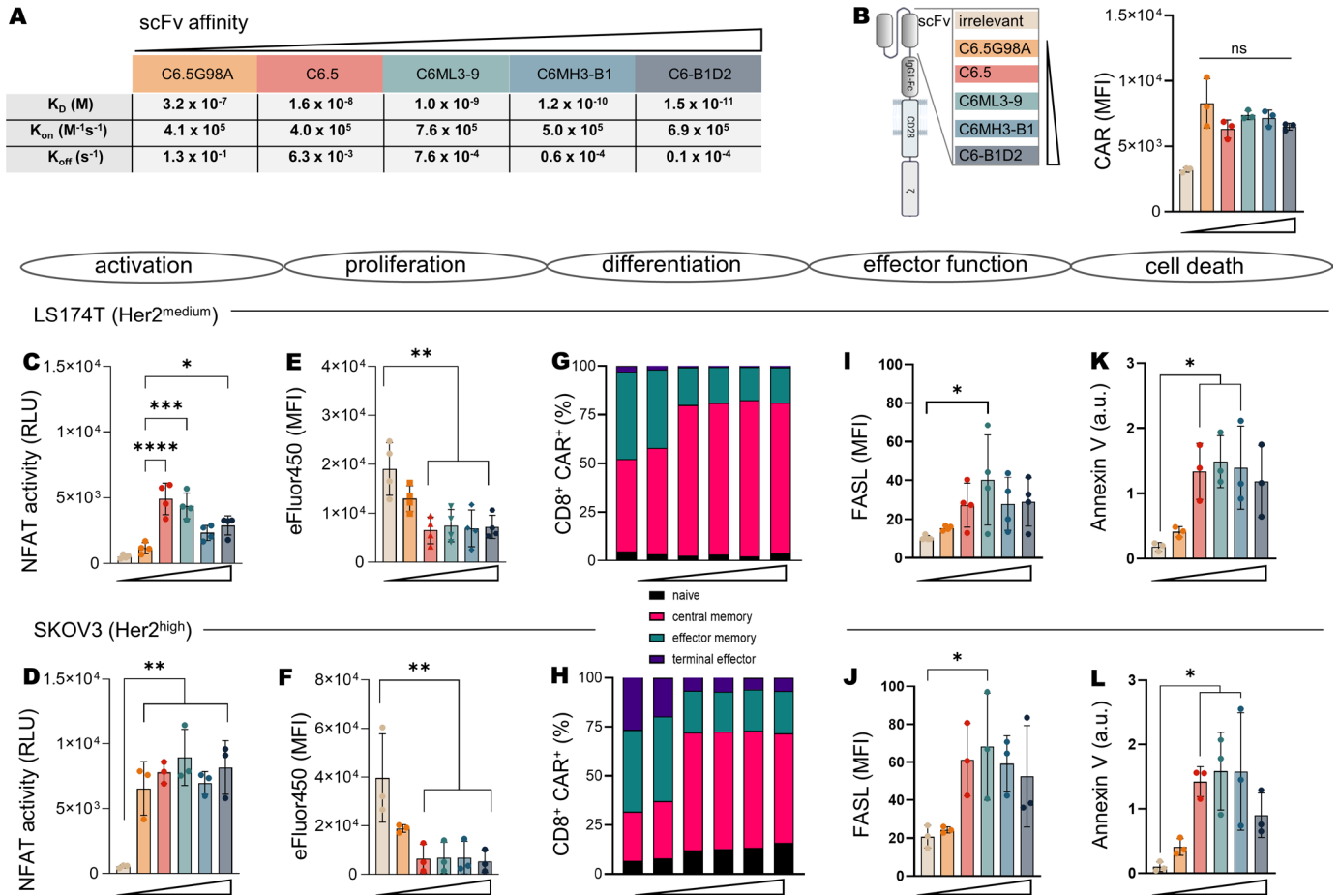


Figure 1 Primary functional capacities of C6.5 derived CAR T cells. (A) Affinities of Her2-specific C6.5 scFv mutants as previously determined by surface plasmon resonance (SPR) using BiAcore.²⁸ (B) scFvs were integrated into a second generation CAR harboring a human IgG1 hinge, CD28 transmembrane and costimulatory, and CD3 signaling domain. CAR expression level on human peripheral blood T cells was assessed by flow cytometry; data represent the geometric mean of the mean fluorescent intensity (MFI) for n=3 donors. CAR graphics: Created in BioRender. Abken, H. (2024) <https://BioRender.com/y88w452>. 1×10^5 T cells were co-incubated with 2×10^4 Her2^{medium} LS174T cells (C, E, G, I, K) or 2×10^4 Her2^{high} SKOV3 cells (D, F, H, J, L). (C, D) CAR-mediated T cell activation strength was evaluated by the Jurkat-Lucia NFAT reporter cell line engineered with the respective Her2 CAR at similar CAR expression levels. Bioluminescence was recorded as relative light units (RLU) after 20 hours of co-incubation with the respective Her2⁺ target cells. Data represent means \pm SD of n=4 (C) or n=3 (D) independent experiments. (E, F) CD8⁺ CAR⁺ T cell proliferation was monitored by recording proliferation dye eFluor™ 450 dilution after 5 days of co-culture with target cells. (G, H) CD8⁺ CAR⁺ T cell subsets after 72 hours of co-culture were determined by flow cytometry (naïve: CD45RO⁻ CD62L⁺; CM: CD45RO⁺ CD62L⁺; EM: CD45RO⁺ CD62L⁻; E: CD45RO⁻ CD62L⁻). (I, J) FASL expression after 72 hours of co-culture of CD8⁺ CAR^{high} CD45RO⁺ CD62L⁺ CAR⁺ T cells with target cells. (K, L) Annexin V staining after 72 hours of co-culture of CD8⁺ CAR⁺ T cells with target cells. Annexin V MFI for each CAR T cell was normalized to the mean MFI of each individual donor. Data represent means \pm SD of n \geq 3 donors. One-way analysis of variance was performed with Tukey's multiple comparison correction. ns (not significant); *p<0.05; **p<0.01; ***p<0.001; ****p<0.0001. CM, central memory; E, effector; EM, effector memory.

the highest affinity scFv. The same scFv showed the strongest antigen non-specific binding compared with the scFvs of lower affinities (figure 2D, online supplemental figures 3–5).

CAR T cell avidity and motility both increased in a non-linear fashion above affinity threshold

To monitor the impact of scFv affinity maturation on CAR T cell avidity, we recorded the binding strength of anti-Her2 CAR T cells to a monolayer of Her2⁺ cancer cells using z-Movi technology (figure 3A,B). Five min of

incubation of CAR T cells with Her2⁺ cells was sufficient to reach a plateau in the contact strength of CAR T cells to target cells (figure 3B). The number of bound CAR T cells was clearly dependent on the binding affinity within a certain range; T cells with a CAR of higher affinity up to a K_D of 1.2×10^{-10} M bound more tightly to target cells than CAR T cells with lower affinity. Unexpectedly, T cells with a CAR within the medium affinity range bound superior compared with the lowest and highest affinity CAR T cells (figure 3C,D). T cells with the highest affinity CAR bound with the same strength as T cells with CARs with lower

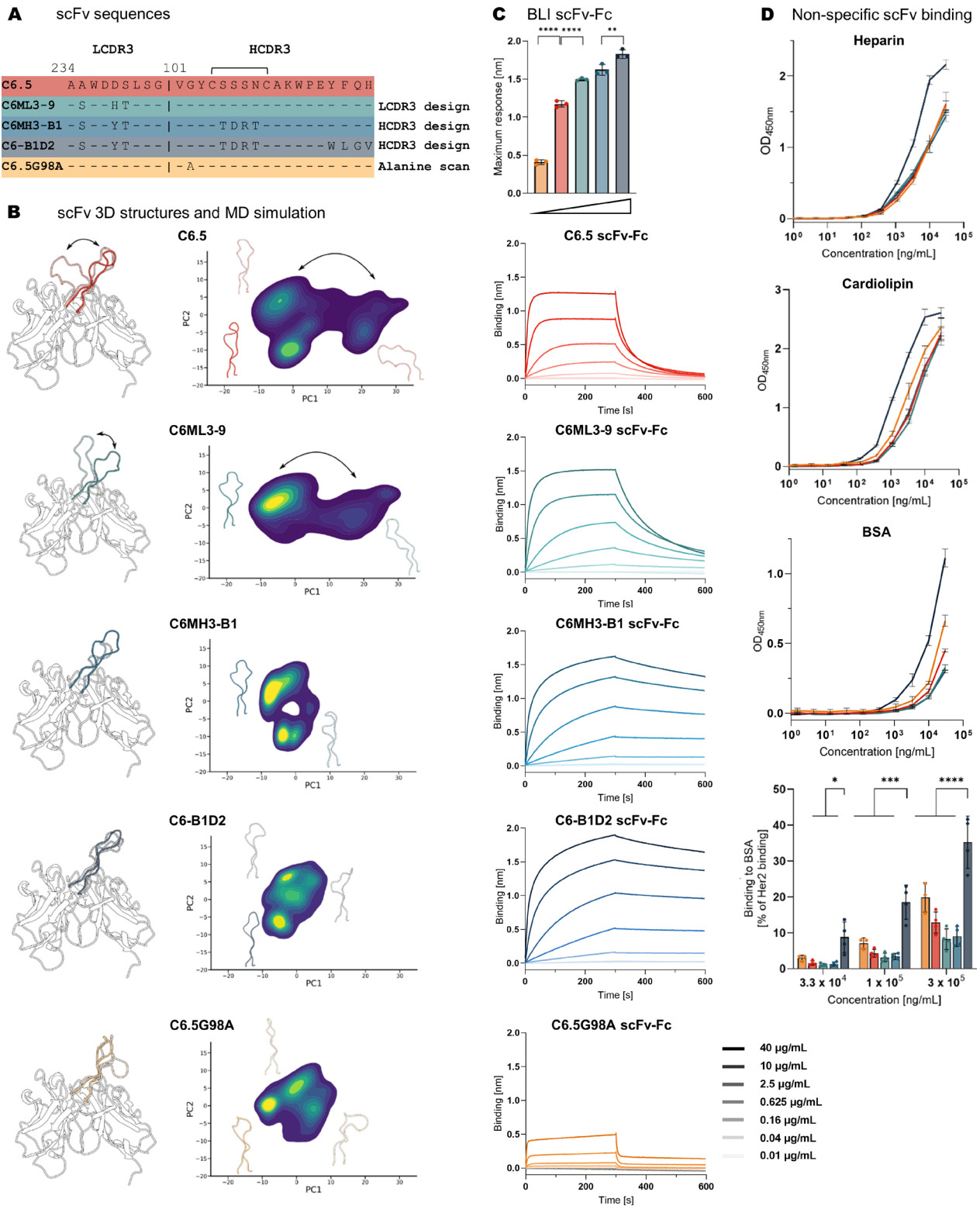


Figure 2 C6.5 derived scFv variants with different affinities differ in their antigen-specific and antigen-independent binding properties. (A) Sequences of the Her2-specific C6.5 scFv mutants previously generated by site-directed mutagenesis.²⁸ (B) Conformations of V_H CDR3 loops of the C6.5 derived scFv panel were evaluated by MD simulation and PCA to analyze conformational states of the loop. (C) scFv binding kinetics were characterized in BLI and are shown as association and dissociation of Her2 protein to/from the immobilized scFv. One representative of a total of three independent experiments is shown. The maximum response is represented as a parameter for affinity. Data represent mean \pm SD of $n=3$. (D) ELISA-based quantification of Her2 independent scFv binding to plate-coated irrelevant antigens heparin, cardiolipin, and bovine serum albumin (BSA). One representative of $n=3$ is shown. Binding to BSA is shown relative to Her2-specific binding. Data represent mean \pm SD of $n=3$. One-way analysis of variance was performed with Tukey's multiple comparison test. * $p<0.05$; ** $p<0.01$; *** $p<0.001$; **** $p<0.0001$. BLI, biolayer interferometry; MD, molecular dynamic; PCA, principal component analysis.

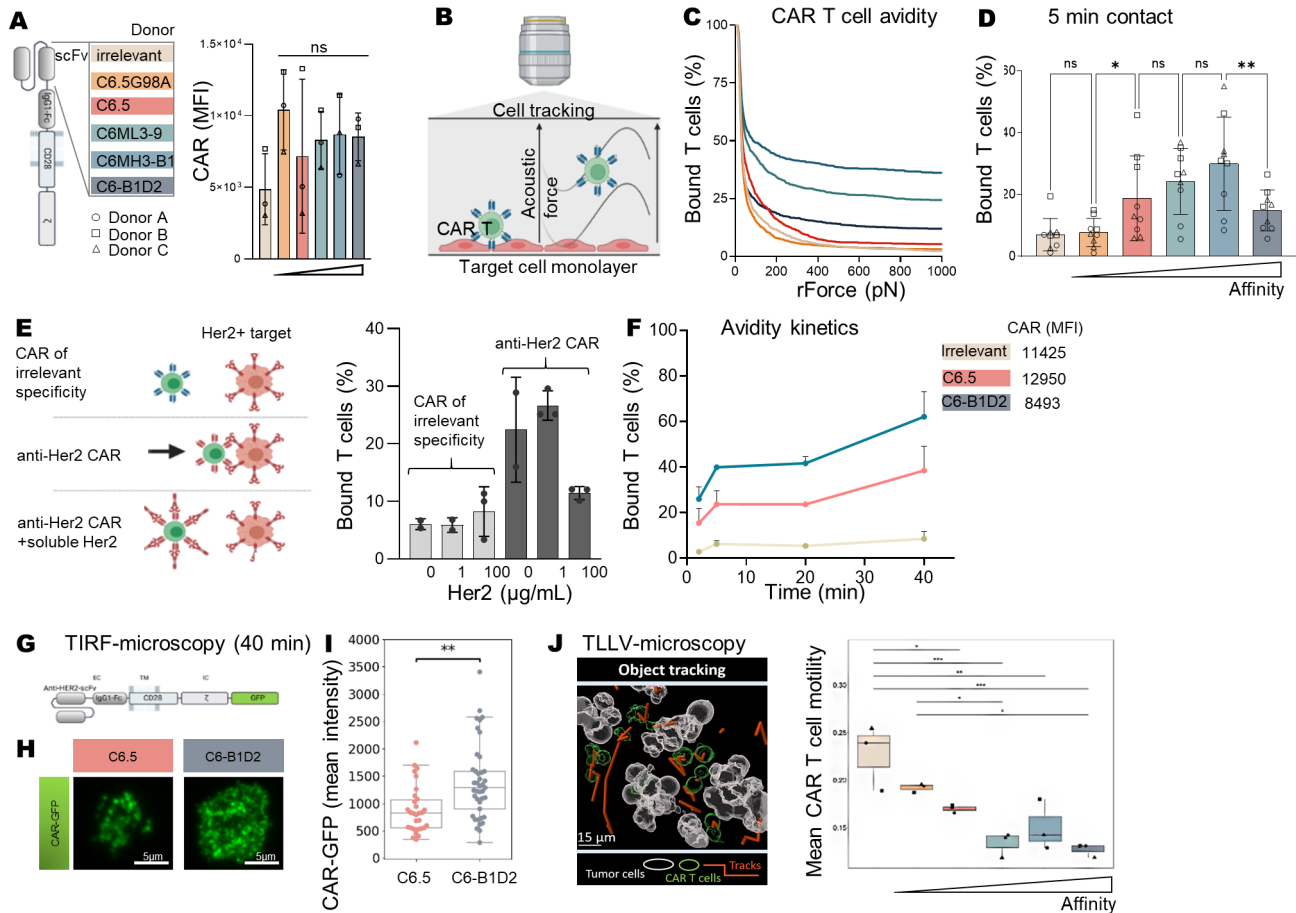


Figure 3 Non-linear correlation between scFv affinity and CAR T cell avidity. (A) The expression levels of Her2 CARs and of the CD30 CAR of irrelevant specificity on engineered T cells; data represent the geometric mean of the mean fluorescence intensity (MFI), $n=3$ donors. CAR graphics (A,G): Created in BioRender. Abken, H. (2024) <https://BioRender.com/y88w452>. (B) CAR T cell binding force on a Her2^{high} SKOV3 cell monolayer as determined by z-Movi avidity analysis. Graphics: Created in BioRender. Abken, H. (2024) <https://BioRender.com/b81y849>. (C) Force ramp applied after 5 min CAR T cell co-incubation with SKOV3 cells. Detachment curve of CAR T cells displayed as mean values of $n=3$ technical replicates (3 runs on 3 different chips per experimental group), data for one representative donor are shown. (D) Collated data of $n=3$ technical replicates of $n=3$ donors ($n=9$ runs on $n=9$ chips total per experimental group); data represent the percentage of T cells bound at plateau force. (E) Soluble Her2 protein at increasing concentration was added to Her2 CAR (C6MH3-B1) and CD30 CAR T cells; data represent the percentage of CAR T cells at the end of force ramp \pm SD, $n=3$ technical replicates ($n=1$ donor). Graphics: Created in BioRender. Barden, M. (2024) <https://BioRender.com/q55q213>. (F) Percentage of CAR T cells bound after 2, 5, 20, and 40 min; representative data for 1 out of 3 donors are displayed. (G–I) T cells were engineered with the CAR-GFP CAR, incubated on Her2 coated plates, and imaged by TIRF microscopy. (I) Data show the mean fluorescence signal per single cell in the contact region with Her2 after 40 min, $n \geq 30$ cells for one donor. Wilcoxon-Mann-Whitney test was performed. (J) Mean CAR T cell motility measured by timelapse-live video (TLLV) microscopy over a time-course of 12.5 hours, $n=3$ donors. Box plots display IQR and median. One-way ANOVA with post hoc Tukey's HSD test was performed to identify significant group differences. (A, D, J). ns (not significant); * $p < 0.05$; ** $p < 0.01$; *** $p < 0.001$; **** $p < 0.0001$. ANOVA, analysis of variance; HSD, honestly significant difference; TIRF, total internal reflection fluorescence.

affinities; binding of the lowest affinity CAR was similar to the binding of CAR T cells of irrelevant specificity. CAR binding forces were specifically mediated by the scFv engagement of Her2 on target cells since the addition of soluble Her2 protein reduced binding down to background levels as observed with CAR T cells of irrelevant specificity (figure 3E).

We assumed that the degree of CAR recruitment depends on the K_{on}/K_{off} values reflecting the probability of binding to and detaching from the cognate antigen when recorded after 5 min when the CAR-target contact

was formed (figure 3D). After prolonged incubation with the target cell monolayer, the CAR with the highest affinity (C6-B1D2 CAR) showed increased binding strength which is in line with its low K_{off} (figure 3F). During the process of contact formation with the respective target cell, CAR molecules are recruited toward the contact zone. CAR molecules involved in interactions with antigen in the contact zone over time may constitute only a subset of CAR molecules present on the T cell surface. We, therefore, recorded CAR recruitment to the contact zone dependent on the binding affinity using TIRF microscopy.

T cells were engineered with a respective panel of CARs that are intracellularly linked to GFP to allow antibody-independent visualization (figure 3G–I). The CAR with the highest affinity (C6-B1D2 CAR) showed more signal of labeled molecules in the contact zone than did the CAR with medium affinity (C6.5 CAR), demonstrating that a high affinity CAR is more efficiently recruited into the contact zone, providing more antigen binders and potentially stronger downstream signaling.

We asked whether different CAR T cell avidities result in different CAR T cell motilities or times in contact to target cells. By implementing time lapse live video microscopy and algorithm-based tracking of CAR T cells, we revealed that increasing CAR binding affinity decreased CAR T cell motility in the presence of an excess of target cells (figure 3J). CAR T cells with the three highest binding affinities produced similarly low CAR T cell motilities, substantially lower than the CARs of medium and low affinities. Our results suggest that high affinity CARs are more efficiently recruited into the contact zone which is associated with longer contact times of CAR T cells to target cells and decreased CAR T cell motility compared with low affinity CARs.

Her2 CARs with high affinity were superior to low/medium affinity CARs in repetitive target cell killing and in elimination of xenograft tumors

While primary activation by CAR T cells depends on binding affinity above threshold (figure 1C,D), we asked whether an increase in avidity also shows superiority under conditions of repetitive antigen engagement simulating tumor conditions with an excess of antigen (“stress test”). T cells engineered with the affinity panel of anti-Her2 CARs were incubated with LS174T cancer cells with medium Her2 levels and SKOV3 cancer cells with high Her2 levels, respectively, for 3 or 4 days. CAR T cells and cancer cells were counted, and the initial number of cancer cells was added again for the next round of stimulation (figure 4A). A CAR of irrelevant specificity served as control. Initially, CAR T cells, except for low affinity CAR T cells, efficiently eliminated cancer cells with high or medium Her2 levels; low affinity C6.5G98A scFv CAR T cells failed to control cancer cell growth from the beginning (figure 4B), likely not reaching the minimum activation threshold. After five or more rounds of stimulation, CAR T cells in all groups lost their killing capacity (figure 4B,E). Medium affinity C6.5 scFv CAR T cells controlled LS174T cancer cell amplification until the end of round 3, after which the killing capacity was lost. The C6ML3-9 scFv CAR with moderately increased affinity provided only minor advantages over the C6.5 scFv CAR whereas high affinity CAR T cells with the C6MH3-B1 and C6-B1D2 scFv provided prolonged cancer cell control outperforming C6.5 scFv CAR T cells. CAR T cells expanded to some degree during the first round of stimulation with Her2^{medium} LS174T cells, but CAR T cell numbers decreased after round 2 (figure 4C). Engagement with Her2^{high} SKOV3 cells resulted in a decrease in

CAR T cell numbers from the first round on; moreover, the low affinity CAR T cells did not decrease in number (figure 4F). With multiple rounds of stimulation, the number of CAR molecules per T cell was downregulated, likely due to CAR internalization on antigen engagement and/or trogocytosis to target cells. Unexpectedly, CARs with high affinity remained at high levels on Her2^{medium} cancer cell engagement throughout all restimulation rounds (figure 4D); CAR levels were even more reduced on engagement of SKOV3 cells with high Her2 levels (figure 4G).

To address how the different killing capacities toward cancer cells in vitro translate to tumor control, NSG mice were engrafted with Her2^{high} N87 tumors²⁹ and CAR T cells were applied at low doses intravenously on day 14 when tumors were fairly established (figure 4H). T cells with the highest affinity C6-B1D2 CAR significantly outperformed T cells with the lower affinity C6.5 CAR in controlling tumor progression, which was also substantiated by improved survival of tumor-bearing mice.

scFv affinity tuning affected both antigen-dependent and antigen-independent CAR signaling

We asked how CAR triggered T cell functionality correlates with scFv intrinsic properties, such as homomerization and oligomerization, which are suggested to contribute to spontaneous CAR clustering and ultimately antigen binding-independent “tonic” signaling.³⁰ In line with non-specific binding of the C6-B1D2 scFv (figure 2D), the C6-B1D2 CAR showed high spontaneous CAR clustering on the T cell surface independent of antigen engagement (figure 5A). NFAT activation, an indicator for downstream signaling, also increased with the C6-B1D2 CAR (figure 5B) indicating spontaneous tonic CAR signaling. The CAR number on cell surface was nearly the same for the entire CAR panel, thus is unlikely a confounding factor (online supplemental figure 1). CD3/CD28 stimulation induced NFAT activation which further increased with the affinity of the expressed CAR (figure 5C), indicating that TCR/CD28 stimulation and tonic CAR signaling cooperate in downstream signaling. For comparison, antigen-induced CAR signaling by adding Her2-Fc protein increased NFAT activation in a dose-dependent fashion; expectedly, NFAT activation increased with scFv binding affinity to Her2 (figure 5D). Taken together, antigen-induced NFAT activity increased with scFv affinity, however, the contribution of scFv intrinsic, antigen-independent NFAT activation was altered by the scFv affinity (figure 5D).

Recently, a correlation between patches of positively charged amino acids and tonic signaling was proposed.³¹ Even though in the case of the C6-B1D2 scFv CAR non-specific scFv-binding and tonic signaling seems to be mainly due to the mutational introduction of hydrophobic, non-polar amino acids into the CDR3 of the scFv heavy chain, the respective mutations could still affect the distribution and functional availability of the positively charged patches (PCPs) on the scFv's surface. We,

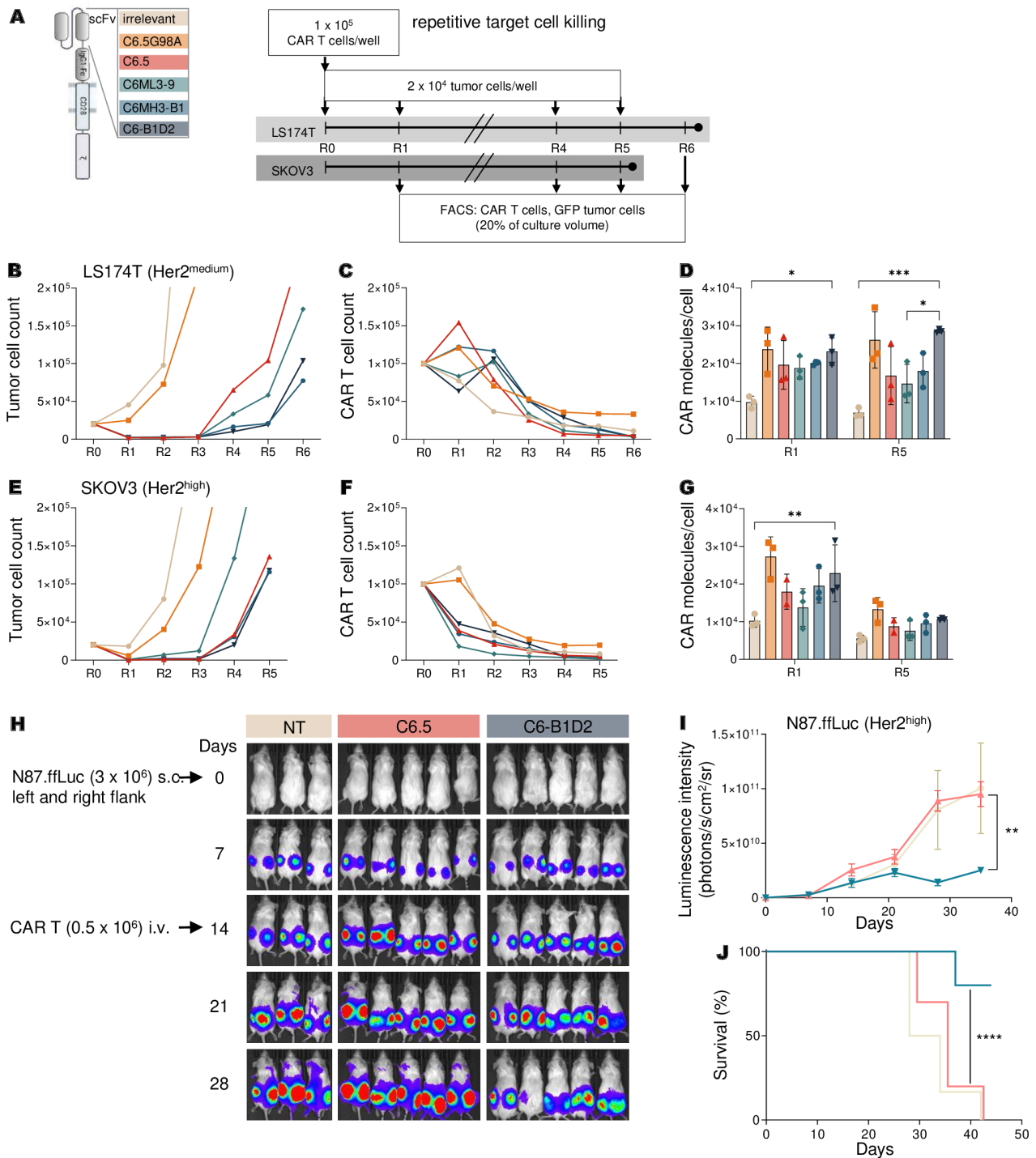


Figure 4 High affinity Her2 CAR T cells provide a prolonged antitumor response in vitro and in vivo. CAR graphics: Created in BioRender. Abken, H. (2024) <https://BioRender.com/y88w452>. (A) Her2 CAR T cells (1×10^5) and control CAR T cells of irrelevant specificity (CD19 CAR) were repetitively stimulated with Her2^{medium} LS174T or Her2^{high} SKOV3 cells (2×10^4) until cancer cell outgrowth (R6 and R5). After each round of co-culture (ie, after 3 or 4 days), 10% of culture volume was removed for flow cytometric quantitation of cell numbers and CAR surface expression. (B) Frequencies of LS174T cells, (C) CAR T cells co-cultured with LS174T cells, (E) SKOV3 cells, (F) CAR T cells co-cultured with SKOV3 cells were determined by flow cytometry using counting beads. Data represent mean values of $n=3$ healthy T cell donors. (D, G) CAR molecules per cell were estimated by flow cytometry using PE quantitation beads. Data represent mean \pm SD of $n=3$ healthy donors. (H) NSG mice were s.c. injected with Her2^{high} N87.ffLuc (3×10^6) cells. On day 14 mice received one intravenous dose of non-modified T cells (NT) (5×10^5 , $n=3$, beige line), or C6.5 scFv CAR T cells (5×10^5 , $n=5$, pink line), or C6-B1D2 scFv CAR T cells (5×10^5 , $n=5$, grey-blue line). Bioluminescence imaging was performed weekly. (I) Tumor growth was monitored by luminescence intensity recording (photons/s/cm²/sr). Graphs represent mean values \pm SD. (J) Percent survival of mice is shown as Kaplan-Meier curve; Log-rank (Mantel-Cox) test was applied for analysis. Two-way ANOVA (D, G) or one-way ANOVA (I) was performed with Tukey's (D, G) or Bonferroni's (I) multiple comparison correction. * $p < 0.05$; ** $p < 0.01$; *** $p < 0.001$; **** $p < 0.0001$. ANOVA, analysis of variance.

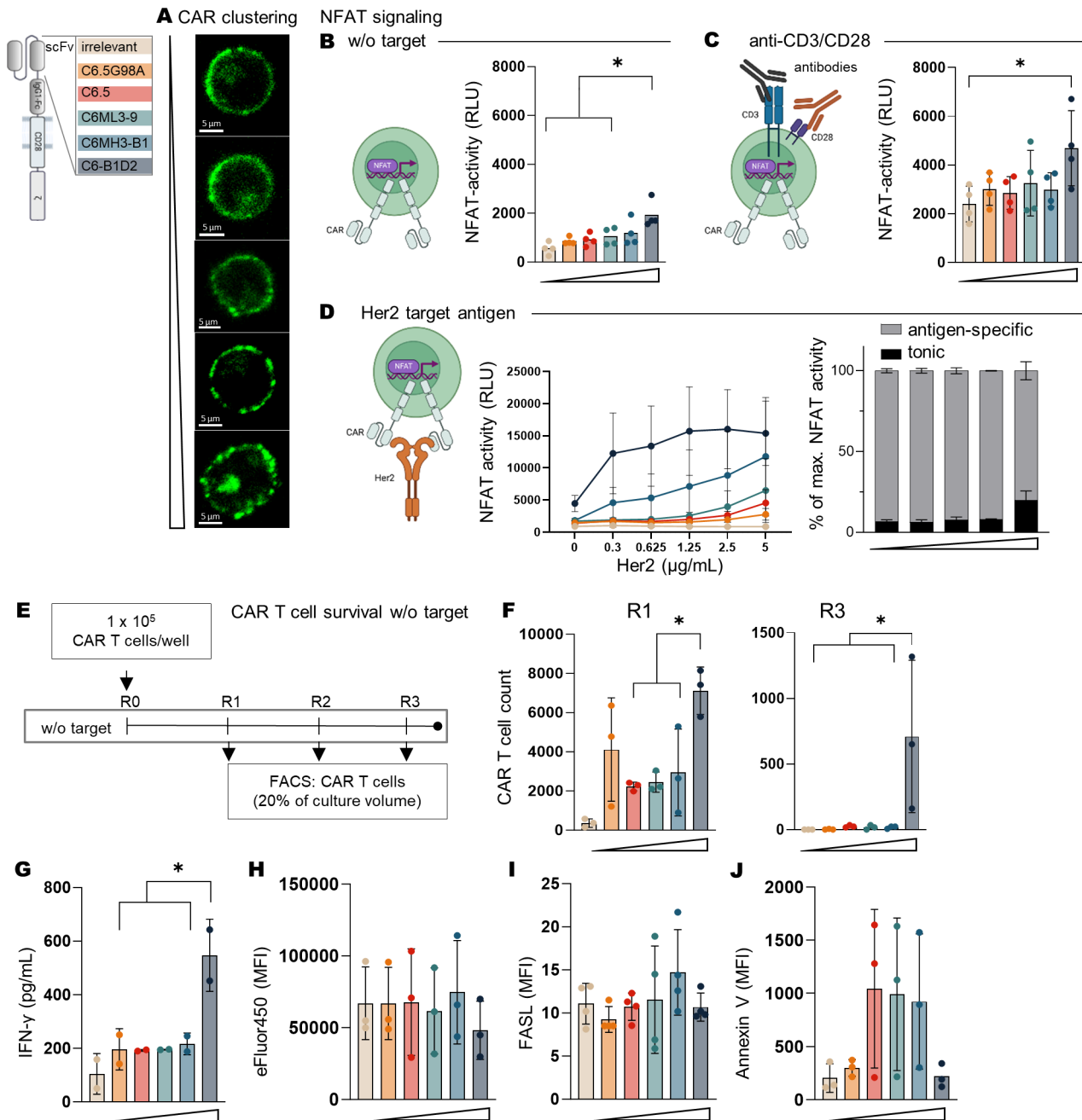


Figure 5 C6-B1D2 scFv CAR clustering and tonic NFAT signaling enhances CAR T cell persistence in the absence of target antigen. (A) CAR clustering was analyzed by confocal imaging of unstimulated CAR-GFP engineered SupT1 cells (n=15). (B–D) CAR mediated T cell activation strength was evaluated by the Jurkat-Lucia NFAT reporter cell line transduced with the respective Her2 CAR and expressed at similar CAR levels. Bioluminescence readout was performed after 20 hours of co-incubation. Data represent means±SD of n=4 (C) or n=3 (D) independent experiments. 1×10⁶ CAR T cells were incubated (B) without stimulation, (C) with anti-CD3 and anti-CD28 antibody stimulation, (D) or with increasing concentrations of plate-coated Her2 protein. Percentages of tonic and antigen-specific signals were calculated based on maximum NFAT value in the entire experiment. (E, F) 1×10⁶ CAR T cells were incubated without antigen. Every 3 days, 20% of the culture volume was taken for flow cytometric recording of T cell counts. (G) IFN-γ was measured by ELISA after 24 hours of co-incubation of CAR T cells with target cells. Data represent means±SD of n=2 donors. (H) CD8⁺ CAR⁺ T cell proliferation was evaluated by proliferation dye eFluor 450 dilution after 72 hours co-culture. (I) FASL was recorded after 72 hours co-culture CD8⁺ CAR^{high} CD45RO⁺ CD62L⁺ CAR⁺ T cells. (J) Annexin V staining after 72 hours co-culture of CD8⁺ CAR⁺ T cells. CAR graphics: Created in BioRender. Abken, H. (2024) <https://BioRender.com/y88w452>. CAR T cell graphics (B–D): Created in BioRender. Abken, H. (2024) <https://BioRender.com/k79o277>. Data represent means±SD of n≥3 donors. One-way ANOVA was performed with Tukey's multiple comparison correction (B–E). ns (not significant); *p<0.05. ANOVA, analysis of variance.

therefore, calculated the PCP score of the scFv constructs as previously described using the Swiss-Model and BindUP web server.^{31–33} Interestingly, we received PCP scores in the range of 40–58 for all constructs (online supplemental table 1) with C6MH3-B1 scFv having the highest score. The score of C6-B1D2 scFv (52) is still in the range that was considered optimal by the authors (46–56),³⁴ however, there was no general correlation between PCP scores and antigen-independent NFAT activation as primary indicator for CAR tonic signaling (figure 5D). Further, tonic signaling induced spontaneous T cell proliferation triggered by the C6-B1D2 scFv CAR was not reduced under high salt conditions (online supplemental figure 6), as previously described for PCPs in the anti-CSPG4 and anti-GD2 CARs.³¹

In regard to functional relevance of tonic signaling, we assumed that an increase in tonic CAR signaling may sustain long-term survival of CAR T cells. To test this hypothesis, we incubated T cells with CARs of different affinities for several rounds in the absence of target cells (figure 5E). After the first round, and more pronounced after the third round, T cells with the high affinity C6-B1D2 scFv CAR survived in a greater proportion than T cells with the lower affinity CARs that were no longer detected after the third round (figure 5F). These findings were substantiated by the increase in IFN- γ release (figure 5G), higher spontaneous proliferation rate of T cells with the highest affinity CAR (figure 5H), unaffected FASL expression (figure 5I), and less spontaneous Annexin V signal indicating lower rate in apoptosis (figure 5J), as compared with the other CARs above affinity threshold.

Tonic CAR signaling and antigen-triggered signaling contribute in a non-additive fashion

To address the impact of CAR clustering on CAR signaling in the absence of antigen, we incubated CAR T cells with increasing concentrations of an anti-IgG antibody that crosslinks the CAR independently of antigen affinity by binding to the extracellular IgG1 CH2-CH3 spacer domain. NFAT activity induced by the C6-B1D2 scFv CAR was elevated at baseline in absence of the anti-IgG antibody (figure 6A, tonic signaling level indicated by dotted line). With increasing anti-IgG antibody concentration, NFAT activity for the C6.5 scFv CAR was raised to the tonic signaling level of the C6-B1D2 CAR and beyond (figure 6A). The same effect was observed for the other anti-Her2 CARs (online supplemental figure 7). Even though anti-IgG CAR crosslinking mechanistically differs from antigen-scFv triggered CAR clustering, by achieving quantitatively similar levels of NFAT activity this model enabled us to study general effects of CAR clustering on CAR T cell functionality. After four rounds of restimulation through low-dose clustering through the IgG1 spacer domain (figure 6B), predominantly CD4⁺ CAR T cells with the highest affinity and highest tonic signaling scFv were amplified up to fivefold whereas the CD8⁺ CAR T cells were not (figure 6C–F). For control, the number of CAR molecules per T cell did not substantially change

on anti-IgG1 antibody mediated CAR clustering (online supplemental figure 8).

Adding Her2 increased NFAT signaling in CAR T cells in a dose-dependent fashion, which was expectedly more pronounced in T cells with higher affinity CARs than in those with medium affinity CARs (figure 6G–I and cf figure 5D). Notably, adding increasing Her2 doses while forcing CAR pre-clustering through an anti-IgG antibody did not further increase NFAT signaling in either high or medium affinity CARs. NFAT activation could not be increased above highest level obtained either by highest antigen-independent clustering or by highest antigen dose. Data indicate that Her2 mediated and spontaneous clustering can complement in a dose dependent fashion up to a cell-intrinsic, maximum level of downstream signaling. The absolute NFAT level, however, depends on an intrinsic scFv property being more pronounced with the high affinity C6-B1D2 scFv than the medium affinity C6.5 scFv. Taken together, these data support our conclusion that in the highest affinity C6-B1D2 CAR both the antigen-mediated and the antigen-independent tonic downstream signaling integrate in increasing the degree of T cell activation.

DISCUSSION

Strength of CAR mediated T cell activation is defined by a complex matrix of dependencies. In this study, we set out to optimize CAR T cell activation and finally antitumor effector functions by a rational CAR design. For a CAR panel targeting the same epitope and having the same CAR expression level, we leveraged an integrative pipeline bridging the gap between CAR scFv affinity maturation and CAR T cell functional capacities.

Our analyses confirmed previous observations that productive CAR triggered T cell activation requires a binding affinity to cognate antigen above threshold to result in T cell downstream signaling, including NFAT activation, and T cell effector functions and expansion, thereby furthermore amplifying the antitumor response.⁶ In the initial round of killing, low affinity anti-Her2 CAR T cells eliminated SKOV3 cells with high Her2 levels as efficiently as did CAR T cells of higher affinity, however, the same low affinity CAR T cells failed to deliver a persisting antitumor response on repetitive engagement of target cells due to insufficiently maintaining the activation strength. This was not the case for high affinity CAR T cells, indicating that differences in overall functional capacities become visible under repetitive antigen engagement, which provokes CAR T cell amplification and survival. Although it remains challenging to define an upper and lower affinity threshold in general, recording both cellular avidity and the signaling strength of each individual CAR under standardized conditions allows narrowing down a window of productive activation.

This study identifies an additional layer of complexity in the matrix controlling T cell effector functions. We revealed that adjusting antigen-triggered CAR T cell activation by

CAR T cell survival upon CAR crosslinking

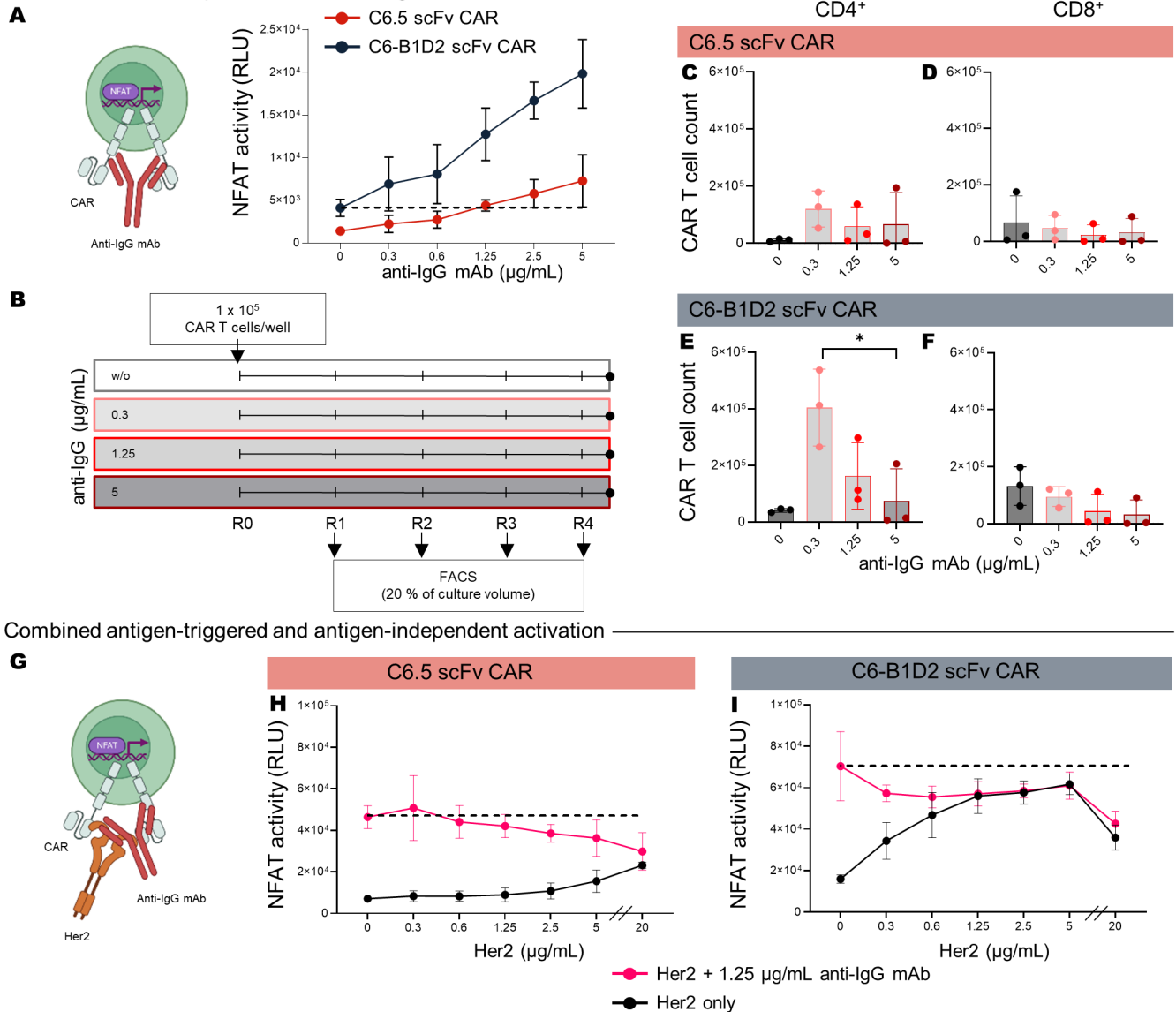


Figure 6 Antigen-independent CAR signaling leads to expansion of CD4⁺ CART cells and allows for combinatorial signaling. CAR T cell graphics: Created in BioRender. Abken, H. (2024) <https://BioRender.com/p11r349>. (A) Anti-IgG crosslinking induced T cell activation strength was evaluated by the Jurkat-Lucia NFAT reporter cell line transduced with the respective Her2 CAR and expressed at similar CAR levels. Bioluminescence readout was performed after 20 hours of co-incubation. Data represent means \pm SD of $n=3$ independent experiments. Based on [figure 6A](#) data, we selected the anti-IgG antibody concentrations used in the CAR T cell survival determination ([figure 6B–F](#)) and for the combined antigen-triggered and antigen-independent activation ([figure 6G–I](#)). (B–F) T cells with C6.5 scFv CAR and C6-B1D2 scFv CAR, respectively, (1×10^6 CAR⁺ T cells/well) were incubated on a 96-well plate over four rounds (3–4 days each round). CARs were antigen-independently crosslinked by a plate-coated anti-IgG antibody that binds to the extracellular IgG1 spacer. CD4⁺ CAR T cell counts (C, E) and CD8⁺ CAR T cell counts (D, F) were recorded by flow cytometry using counting beads. CAR T cell counts after round 4 (R4) are displayed. (G–I) CAR mediated T cell activation strength was evaluated by the Jurkat-Lucia NFAT reporter cell line engineered with the respective Her2 CAR and expressed at similar CAR levels. Bioluminescence was recorded after 20 hours of co-incubation. 1×10^6 CAR T cells were incubated with increasing concentrations of plate-coated Her2 protein with or without anti-IgG antibody. Data represent means \pm SD of $n \geq 2$ independent experiments. Statistical calculation was done by ANOVA with Tukey’s multiple comparison correction. * $p < 0.05$. ANOVA, analysis of variance.

scFv affinity maturation was accompanied by an increase in antigen-independent “tonic” activation strength, which is an intrinsic property of the scFv.¹⁶ Exchange of individual amino acids in the CDR of the Ig heavy or light chain substantially altered the antigen-independent, tonic strength of the respective CAR ([figure 5](#)) which is in accordance with

previous observations with another CAR.¹⁵ Our data furthermore indicate that antigen-independent scFv binding is associated with tonic signaling. In the case of the C6-B1D2 scFv CAR, tonic signaling seems to be driven by hydrophobic interactions of the scFv and is unlikely to be primarily due to the scFv’s positive charge. While the analyzed scFvs have

a similar PCP score, tonic signaling by the respective CAR is strikingly different (online supplemental table 1; figure 5). The increase of tonic signaling appears to be a side effect of affinity maturation rather than being in direct correlation with affinity. Notably, the molecular basis of tonic signaling may be different for each scFv in the same CAR backbone. Tonic signaling may additionally be due to a short linker,³⁵ to CDR clustering,¹⁶ or due to clustering with other molecules on the T cell surface, like heterodimerization of CD28 CARs with the T cell endogenous CD28.³⁶

Tonic signaling triggered by the CAR underlies the same T cell intrinsic regulatory mechanisms as antigen-specific CAR signaling. The FDA recently reported cases of secondary malignancies after CAR T cell treatment which are potentially caused by mutations of nuclear genes such as TET2, NFKB2, PTPRB and/or JAK3.³⁷ In this context, it remains unclear how tonic CAR signaling would affect a T cell clone with a pre-existing mutational load and malignant potential. As long as the T cells' regulatory mechanisms are in place, excessive tonic signaling through the CAR drives the T cell into exhaustion,^{14,38} therefore, seems to be "self-limiting" and is not expected to cause secondary CAR T cell malignancies. Noteworthy, tonic signaling can be beneficial to the CAR T cell therapeutic efficacy as the high affinity CAR with elevated tonic signaling was superior in sustaining CAR T cell amplification, tumor control, and survival without showing signs of malignant transformation.

Taken together, our findings draw a caveat with the current dogma of improving CAR T cell functionality and safety exclusively by decreasing CAR affinity and tonic signaling which may result in diminished CAR T cell survival on prolonged antigen exposure. Antigen-triggered and tonic signaling seem to be associated and need to be adjusted in an integrative manner to augment CAR T cell efficacy in the context of repetitive antigen encounter in the response toward solid tumors.

Author affiliations

¹Division of Genetic Immunotherapy, Leibniz Institute for Immunotherapy, Regensburg, Germany

²Institute for Drug Discovery, Leipzig University Faculty of Medicine, Leipzig, Germany

³Center for Scalable Data Analytics and Artificial Intelligence, ScaDS.AI, Dresden/Leipzig, Germany

⁴Institute of Applied Physics, TU Wien, Vienna, Austria

⁵Department of Biophysics and Cell Biology, University of Debrecen Faculty of Medicine, Debrecen, Hungary

⁶Department of Health Technology, Technical University of Denmark, Kgs. Lyngby, Denmark

⁷Biophysics and Cell Biology, University of Debrecen, Debrecen, Hungary

⁸Fraunhofer Institute for Cell Therapy and Immunology (IZI), Leipzig, Germany

⁹Department I Internal Medicine, University Hospital Cologne, and Center for Molecular Medicine Cologne, University of Cologne, Cologne, Germany

Acknowledgements We thank Dr. James D. Marks (University of California, San Francisco, CA) for providing the C6.5-derived anti-Her2 scFvs. We further thank Martina Esser, Anja Pavlica and Charlotte Schenkel for excellent technical assistance. Parts of figure 1, 3, 4, 5, and 6 were created with BioRender (biorender.com) for which the authors have a license.

Contributors Conceptualization: MB, AAH, HA. Methodology: MB, PRE, VH, ME, PP, LV, BG, AS, RUWF, VB, DCH, AH. Investigation: MB, PRE, VH, ME, PP, LV, BG, RUWF,

VB, DCH, AH, GJS, AS, GV, CTS, AAH, HA. Visualization: MB, PRE, VH, ME, LV. Funding acquisition: GJS, AS, GV, CTS, HA. Project administration: MB, HA. Supervision: GJS, AS, GV, CTS, HA. Guarantor: HA. Writing—original draft: MB, HA. Writing—review and editing: all authors.

Funding Work in the Abken Lab was supported by Deutsche Forschungsgemeinschaft (DFG, German Research Foundation)—project number 324392634—TRR 221, subproject A02 (PRE). ME and CTS were supported by the Federal Ministry of Education and Research of Germany and by the Sächsische Staatsministerium für Wissenschaft Kultur und Tourismus (SMWK) in the program Center of Excellence for AI-research "Center for Scalable Data Analytics and Artificial Intelligence Dresden/Leipzig" [project identification number ScaDS.AI]. Work in the Schoeder lab was supported by a TG-70 guideline from the SMWK under the award "KI-CAR" (CTS). Work in the Vereb lab was supported by National Research, Development and Innovation Office, Hungary, OTKA K143771 (GV) and FK132773 (AS), Janos Bolyai Research Scholarship of the Hungarian Academy of Sciences (AS), New National Excellence Program of the Ministry for Innovation and Technology UNKP-21-5-DE-482 (AS) and UNKP-22-3-II-DE44 (BG).

Competing interests No, there are no competing interests.

Patient consent for publication Not applicable.

Ethics approval This study involves human participants and blood from healthy donors was obtained under the Ethic approval 21-2224-101, University Hospital Regensburg. The participants provided their written informed consent to participate in this study. Participants gave informed consent to participate in the study before taking part.

Provenance and peer review Not commissioned; externally peer reviewed.

Data availability statement Data are available on reasonable request. All data relevant to the study are included in the article or uploaded as online supplemental information.

Supplemental material This content has been supplied by the author(s). It has not been vetted by BMJ Publishing Group Limited (BMJ) and may not have been peer-reviewed. Any opinions or recommendations discussed are solely those of the author(s) and are not endorsed by BMJ. BMJ disclaims all liability and responsibility arising from any reliance placed on the content. Where the content includes any translated material, BMJ does not warrant the accuracy and reliability of the translations (including but not limited to local regulations, clinical guidelines, terminology, drug names and drug dosages), and is not responsible for any error and/or omissions arising from translation and adaptation or otherwise.

Open access This is an open access article distributed in accordance with the Creative Commons Attribution Non Commercial (CC BY-NC 4.0) license, which permits others to distribute, remix, adapt, build upon this work non-commercially, and license their derivative works on different terms, provided the original work is properly cited, appropriate credit is given, any changes made indicated, and the use is non-commercial. See <http://creativecommons.org/licenses/by-nc/4.0/>.

ORCID iDs

Markus Barden <http://orcid.org/0000-0002-4923-2254>

Patrick Ronan Elsenbroich <http://orcid.org/0009-0006-4466-3895>

Bence Gergely <http://orcid.org/0000-0001-9005-6910>

Andreas A Hombach <http://orcid.org/0000-0001-9328-8442>

REFERENCES

- 1 Good CR, Aznar MA, Kuramitsu S, *et al.* An NK-like CAR T cell transition in CAR T cell dysfunction. *Cell* 2021;184:6081–100.
- 2 Mezösi-Csaplár M, Szóór Á, Vereb G. CD28 and 41BB Costimulatory Domains Alone or in Combination Differentially Influence Cell Surface Dynamics and Organization of Chimeric Antigen Receptors and Early Activation of CAR T Cells. *Cancers (Basel)* 2023;15:3081.
- 3 Mao R, Kong W, He Y. The affinity of antigen-binding domain on the antitumor efficacy of CAR T cells: Moderate is better. *Front Immunol* 2022;13:1032403.
- 4 Rodriguez-Marquez P, Calleja-Cervantes ME, Serrano G, *et al.* CAR density influences antitumoral efficacy of BCMA CAR T cells and correlates with clinical outcome. *Sci Adv* 2022;8:eabo0514.
- 5 Greenman R, Pizem Y, Haus-Cohen M, *et al.* Shaping Functional Avidity of CAR T Cells: Affinity, Avidity, and Antigen Density That Regulate Response. *Mol Cancer Ther* 2021;20:872–84.
- 6 Chmielewski M, Hombach A, Heuser C, *et al.* T cell activation by antibody-like immunoreceptors: increase in affinity of the single-chain fragment domain above threshold does not increase T cell

- activation against antigen-positive target cells but decreases selectivity. *J Immunol* 2004;173:7647–53.
- 7 Zheng L, Ren L, Kouhi A, et al. A Humanized Lym-1 CAR with Novel DAP10/DAP12 Signaling Domains Demonstrates Reduced Tonic Signaling and Increased Antitumor Activity in B-Cell Lymphoma Models. *Clin Cancer Res* 2020;26:3694–706.
 - 8 Hegde M, Joseph SK, Pashankar F, et al. Tumor response and endogenous immune reactivity after administration of HER2 CAR T cells in a child with metastatic rhabdomyosarcoma. *Nat Commun* 2020;11:3549.
 - 9 Vitanza NA, Johnson AJ, Wilson AL, et al. Locoregional infusion of HER2-specific CAR T cells in children and young adults with recurrent or refractory CNS tumors: an interim analysis. *Nat Med* 2021;27:1544–52.
 - 10 Morgan RA, Yang JC, Kitano M, et al. Case report of a serious adverse event following the administration of T cells transduced with a chimeric antigen receptor recognizing ERBB2. *Mol Ther* 2010;18:843–51.
 - 11 Shabaneh TB, Stevens AR, Stull SM, et al. Systemically administered low-affinity HER2 CAR T cells mediate antitumor efficacy without toxicity. *J Immunother Cancer* 2024;12:e008566.
 - 12 Ghorashian S, Kramer AM, Onuoha S, et al. Enhanced CAR T cell expansion and prolonged persistence in pediatric patients with ALL treated with a low-affinity CD19 CAR. *Nat Med* 2019;25:1408–14.
 - 13 Michelozzi IM, Gomez-Castaneda E, Pohle RVC, et al. The Enhanced Functionality of Low-Affinity CD19 CAR T Cells Is Associated with Activation Priming and Polyfunctional Cytokine Phenotype. *Blood* 2020;136:52–3.
 - 14 Long AH, Haso WM, Shern JF, et al. 4-1BB costimulation ameliorates T cell exhaustion induced by tonic signaling of chimeric antigen receptors. *Nat Med* 2015;21:581–90.
 - 15 Zhou J, Shi F, Luo X, et al. The persistence and antitumor efficacy of CAR-T cells are modulated by tonic signaling within the CDR. *Int Immunopharmacol* 2024;126:111239.
 - 16 Sarén T, Saronio G, Marti Torrell P, et al. Complementarity-determining region clustering may cause CAR-T cell dysfunction. *Nat Commun* 2023;14:4732.
 - 17 Landoni E, Fucá G, Wang J, et al. Modifications to the Framework Regions Eliminate Chimeric Antigen Receptor Tonic Signaling. *Cancer Immunol Res* 2021;9:441–53.
 - 18 Jumper J, Evans R, Pritzel A, et al. Highly accurate protein structure prediction with AlphaFold. *Nature New Biol* 2021;596:583–9.
 - 19 Jo S, Kim T, Iyer VG, et al. CHARMM-GUI: a web-based graphical user interface for CHARMM. *J Comput Chem* 2008;29:1859–65.
 - 20 Tian C, Kasavajhala K, Belfon KAA, et al. ff19SB: Amino-Acid-Specific Protein Backbone Parameters Trained against Quantum Mechanics Energy Surfaces in Solution. *J Chem Theory Comput* 2020;16:528–52.
 - 21 Case DA, Cheatham TE III, Darden T, et al. The Amber biomolecular simulation programs. *J Comput Chem* 2005;26:1668–88.
 - 22 Nguyen H, Roe DR, Swails J, et al. PYTRAJ v1.0.0.dev1: Interactive data analysis for molecular dynamics simulations. 2016.
 - 23 Roe DR, Cheatham TEI. PTRAJ and CPPTRAJ: Software for Processing and Analysis of Molecular Dynamics Trajectory Data. *J Chem Theory Comput* 2013;9:3084–95.
 - 24 Golumba-Nagy V, Kuehle J, Abken H. Genetic Modification of T Cells with Chimeric Antigen Receptors: A Laboratory Manual. *Hum Gene Ther Methods* 2017;28:302–9.
 - 25 Schrangl L. sdt-python: python library for fluorescence microscopy data analysis. 2020.
 - 26 Harris CR, Millman KJ, van der Walt SJ, et al. Array programming with NumPy. *Nature New Biol* 2020;585:357–62.
 - 27 Virtanen P, Gommers R, Oliphant TE, et al. SciPy 1.0: fundamental algorithms for scientific computing in Python. *Nat Methods* 2020;17:261–72.
 - 28 Schier R, McCall A, Adams GP, et al. Isolation of picomolar affinity anti-c-erbB-2 single-chain Fv by molecular evolution of the complementarity determining regions in the center of the antibody binding site. *J Mol Biol* 1996;263:551–67.
 - 29 Szöör A, Tóth G, Zsebik B, et al. Trastuzumab derived HER2-specific CARs for the treatment of trastuzumab-resistant breast cancer: CAR T cells penetrate and eradicate tumors that are not accessible to antibodies. *Cancer Lett* 2020;484:1–8.
 - 30 Albert S, Koristka S, Gerbault A, et al. Tonic Signaling and Its Effects on Lymphopoiesis of CAR-Armed Hematopoietic Stem and Progenitor Cells. *J Immunol* 2019;202:1735–46.
 - 31 Chen J, Qiu S, Li W, et al. Tuning charge density of chimeric antigen receptor optimizes tonic signaling and CAR-T cell fitness. *Cell Res* 2023;33:341–54.
 - 32 Waterhouse A, Bertoni M, Bienert S, et al. SWISS-MODEL: homology modelling of protein structures and complexes. *Nucleic Acids Res* 2018;46:W296–303.
 - 33 Paz I, Kligun E, Bengad B, et al. BindUP: a web server for non-homology-based prediction of DNA and RNA binding proteins. *Nucleic Acids Res* 2016;44:W568–74.
 - 34 Qiu S, Chen J, Wu T, et al. CAR-Toner: an AI-driven approach for CAR tonic signaling prediction and optimization. *Cell Res* 2024;34:386–8.
 - 35 Singh N, Frey NV, Engels B, et al. Single Chain Variable Fragment Linker Length Regulates CAR Biology and T Cell Efficacy. *Blood* 2019;134:247.
 - 36 Muller YD, Nguyen DP, Ferreira LMR, et al. The CD28-Transmembrane Domain Mediates Chimeric Antigen Receptor Heterodimerization With CD28. *Front Immunol* 2021;12:639818.
 - 37 Levine BL, Pasquini MC, Connolly JE, et al. Unanswered questions following reports of secondary malignancies after CAR-T cell therapy. *Nat Med* 2024;30:338–41.
 - 38 Lamarche C, Ward-Hartstonge K, Mi T, et al. Tonic-signaling chimeric antigen receptors drive human regulatory T cell exhaustion. *Proc Natl Acad Sci U S A* 2023;120:e2219086120.